Effect of Silica and Alumina Promoters on Co-precipitated Fe-Cu-K Based Catalysts for the Enhancement of CO_2 Utilization during Fischer-Tropsch Synthesis

Mohammad Rafati [a], *Lijun Wang* [b,c*], *Abolghasem Shahbazi* [b, c]

[a] Department of Energy and Environmental Systems

[b] Department of Natural Resources and Environmental Design

[c] Department of Chemical, Biological, and Bioengineering

North Carolina Agricultural and Technical State University, 1601 East Market Street, Greensboro, North Carolina 27411, USA

*Corresponding author, Tel: +1 336 2853833, Fax: +1 336 3347270, Email: lwang@ncat.edu (L.J. Wang)

Abstract

Silica and alumina were used as structural promoters to increase the catalytic activity of a co-precipitated Fe-Cu-K catalyst for the CO_2 and CO hydrogenation during Fischer-Tropsch (FT) synthesis. The doubly-promoted Fe-Cu-K-Si-Al catalyst achieved higher CO and CO_2 conversions than the Fe-Cu-K catalyst and singly-promoted Fe-Cu-K-Al and Fe-Cu-K-Si catalysts. The CO and CO_2 conversions of the syngas with 54%H_2/10%CO/29%CO_2/7%N_2 over the doubly-promoted catalyst were 88.3% and 25.2%, respectively, compared to 81.8% and 18.5% for the Fe-Cu-K catalyst. In this case, the C_{5+} selectivity of the doubly-promoted catalyst was 71.9%, which was slightly lower than 75.5% for the Fe-Cu-K catalyst. The CO_2 was converted to hydrocarbons using the doubly-promoted catalyst when the CO_2/(CO+CO_2) ratio

was higher than 0.35 for H_2-balanced syngas at $H_2/(2CO+3CO_2)=1.0$, and 0.5 for H_2-deficient syngas at $H_2/(2CO+3CO_2)=0.5$). The increase of hydrogen content in the syngas increased the methane selectivity at the expense of decrease in the liquid hydrocarbon selectivity.

Keywords: Catalyst promoter, CO_2 utilization, Fischer-Tropsch, Syngas, Biofuel

1. Introduction

The combination of biomass gasification and subsequent Fischer–Tropsch (FT) synthesis is a promising pathway to produce liquid fuels and chemicals as alternatives to fossil-based counterparts [1-3]. The FT synthesis converts a mixture of H_2 and CO to a wide range of hydrocarbons according to the following reaction:

$$CO + 2H_2 \rightarrow CH_2 + H_2O \quad (FT\ reaction)$$

According to the above reaction, it requires 2 moles of H_2 to convert 1 mole of CO into the precursor of methylene ($-CH_2-$).

Syngas produced through coal and biomass gasification contains a significant amount of CO_2 which typically ranges from 10% to up to 35% depending on the gasification technology and operating conditions [4, 5]. In current industrial FT processes, CO_2 is usually stripped out of the syngas by adsorption such as Rectisol and Selexol prior to the FT synthesis, which causes significant energy loss and typically adds up to 10% additional capital costs and associated operating costs [5]. With increased global concerns and demand for controlling greenhouse gas (GHG) emissions, it is desirable to utilize CO_2 for production of fuels and chemicals, as it accounts for more than 75% of the total GHG emissions [6]. Earlier studies revealed the

possibility of converting CO_2 into hydrocarbons through the reverse water-gas shift (rWGS) reaction and subsequent FT synthesis of formed CO [7-9], which are given by:

$$CO + H_2O \leftrightarrow CO_2 + H_2 \qquad \Delta H° 298 = -41\ kJ.mol^{-1} \qquad (WGS\ reaction)$$

$$CO + 2H_2 \rightarrow CH_2 + H_2O \qquad \Delta H° 298 = -165\ kJ.mol^{-1} \qquad (FT\ reaction)$$

According to the above two reactions, it requires 3 moles of H_2 to convert 1 mole of CO_2 into the precursor of $–CH_2-$. As the WGS reaction is an exothermic and equilibrium–controlled reaction, a high temperature is thermodynamically favorable towards the reverse direction (rWGS) [10]. However, a high equilibrium temperature of rWGS reaction promotes the formation of undesirable methane during FT synthesis [11]. Although the combination of rWGS and FT reactions in a single reactor can reduce the process costs and design complexity, it is critical to design a highly active catalyst that is capable of catalyzing rWGS reaction at a typical temperature of FT synthesis.

Riedel et al. (1999) incorporated a WGS-active component of MnO onto a Co-based catalyst for CO_2 hydrogenation. They concluded that the concentration of CO generated from the CO_2 shift reaction was too low to establish the FT regime on the Co-based catalyst of Co-MnO-Aerosil-Pt [12]. Other studies, however, showed the possibility of using iron-based catalysts for the hydrogenation of CO_2 or a CO/CO_2 mixture into FT hydrocarbons, as iron is active to catalyze both FT and WGS reactions [12-14]. It was reported that potassium promotion is essential to enhance the carburization of an iron-based catalyst for CO_2 hydrogenation [15]. Iron-carbide phases are known to be one of the active phases of an Fe-based catalyst for FT synthesis [12, 16]. The potassium promotion is important to form the surface carbide phases when the CO concentration in a CO_2-containing syngas is low. Excessive potassium, however, should be avoided as it increases the carbon deposition and catalyst deactivation [9, 15].

66

67 Al_2O_3 is an important structural and chemical promoter in hydrogenation of CO_2 over iron-based
68 catalysts [12, 17]. Jun et al. [17] compared the activity and selectivity of Fe-Cu-K-Si and Fe-Cu-
69 K-Al catalysts in FT synthesis with a model biomass-derived syngas. The latter catalyst was able
70 to convert both CO and CO_2 into hydrocarbons, but the former was much less active and
71 achieved a very low conversion efficiency. They hypothesized that high concentrations of CO_2
72 and H_2O inside the reactor created a highly oxidizing environment, which resulted in a very low
73 concentration of iron carbides on the catalyst surface and thus low activity of Fe-Cu-K-Si
74 catalyst. In their study, a binder was used to introduce either SiO_2 or Al_2O_3 to the precipitated
75 active metals. Other studies found that the method used to add SiO_2 or Al_2O_3 had a large impact
76 on the activity and selectivity of the iron-based catalysts for the FT synthesis using CO and H_2
77 syngas [18, 19]. Ding et al. [20] investigated the effect of SiO_2-coating of an FeK/Al_2O_3
78 supported catalyst on its activity and selectivity for CO_2 hydrogenation to hydrocarbons. The
79 addition of SiO_2 was realized by impregnating the calcined catalyst with tetraethyl orthosilicate
80 (TEOS) dissolved in cyclohexane. They found that the optimum amount of SiO_2 coating on the
81 catalyst increased CO_2 conversion and selectivity toward C_{2+} hydrocarbons. It was also reported
82 that an Fe-Cu-K catalyst doubly-promoted with SiO_2 and Al_2O_3 would achieve better activity of
83 FT synthesis than the catalyst singly-promoted by either SiO_2 or Al_2O_3 over H_2/CO syngas [21].
84 However, no research was found on synergetic effect of such catalyst complex in hydrogenation
85 of CO_2 or a CO/CO_2 mixture. The objective of this research was to study the effects of silica and
86 alumina promoters on the activity and selectivity of a co-precipitated Fe-Cu-K based catalyst
87 over syngas with various H_2, CO and CO_2 contents during FT synthesis.
88

2. Experimental

2.1. Catalysts preparation

An Fe-Cu-K complex was synthesized as the base catalyst. Copper was added to facilitate the reduction of iron oxides and a small amount of potassium was added to promote the formation of iron carbides. The catalysts were prepared by the combination of co-precipitation and impregnation methods. An aqueous buffer solution was prepared by adding appropriate amounts of ammonium carbonate, water and nitric acid in a heated reaction vessel. A hot aqueous solution of iron nitrate, aluminum nitrate and/or TEOS dissolved in ethanol was added to the reaction vessel while ammonium carbonate was added in a controlled rate by using a pH controller and peristaltic pumps to maintain the pH of the precipitating solution at 7.0±0.2. The temperature of the precipitating solution was kept at 70±2.0 °C by using a temperature controller. Precipitates were aged at the reaction temperature for 15 minutes, then filtered and washed with distilled water several times, and finally dried at 120 °C for 8 hours followed by calcination at 350 °C for 1 hour. Copper and potassium were, then, added by sequential incipient wetness impregnation of aqueous solutions of copper nitrate and potassium carbonate, respectively. After each impregnation, the catalysts were dried at 120°C for 8 hours. The catalysts were finally calcined at 400 °C for 4 hours. The nominal compositions of synthesized catalysts as well as calculated composition through the ICP and energy-dispersive X-ray spectroscopy (EDX) are given in Table 1.

Table 1. Elemental compositions of calcined catalysts

Catalysts notation	Nominal composition [a]	from ICP-OES	from EDX
Fe-Cu-K	100Fe/2Cu/4K	100Fe/2.1Cu/3.9K	100Fe/2.1Cu/4.1K
Fe-Cu-K-Al	100Fe/2Cu/4K/25Al	100Fe/1.9Cu/4.0/25.1Al	100Fe/2.1Cu/5.1K/18.3Al
Fe-Cu-K-Si	100Fe/2Cu/4K/25Si	100Fe/1.9Cu/4.1K/25.8Si	100Fe/3.6Cu/4.1K/11.6Si

Fe-Cu-K-Si-Al	100Fe/2Cu/4K/10Si/15Al	100Fe/1.9Cu/4.1K/10.2Si/14.9Al	100Fe/2.5Cu/5.6K/4.4Si/10.7Al

[a] *relative composition on atomic basis*

2.2. Catalyst characterization

The BET surface area, pore volume and pore size distribution of the catalysts were determined by a N_2 physical adsorption apparatus (ASAP 2020, Micromeritics, USA). Samples were dried and degassed at 300 °C for 4 hours prior to the N_2 adsorption.

The temperature-programmed reduction (TPR) of the catalysts was carried out with a 10%H_2-90%Ar mixture in a chemisorption instrument (Autochem II 2920, Micromeritics, USA). About 50 mg of sample was dried and degassed at 300°C for 1 hour under a flow of Ar gas prior to the reduction. The temperature and detector signals were then continuously recorded while heating the sample up to 800 °C at 10 °C/min and then keeping at the final temperature for 15 minutes.

For CO_2-temperature programmed desorption (CO_2-TPD), 50 mg of each sample was reduced at 460 °C for 6 hours under a flow of H_2 before carrying out the adsorption. Then, the CO_2 adsorption was done with introducing a flow of CO_2 for 30 minutes, followed by flushing out the weakly adsorbed CO_2 molecules under a flow of He for 30 minutes. Then, the desorption profile was recorded continuously while the temperature was ramped to 900°C at 7°C/min and then kept at the final temperature for 30 minutes under a flow of He at 30 mL/min.

The temperature-programmed decarburization (TPDC) experiments were performed on passivated spent catalysts in the same equipment. About 50 mg of each sample was placed inside

a quartz tube. The temperature was ramped to 800°C at 10°C/min and then kept at the final temperature for 30 minutes under a flow of H_2 at 50 mL/min. The main product of this reaction was methane [9] which was continuously detected by a TCD to generate the TPDC profile.

X-ray diffraction (XRD) measurements were performed to investigate the bulk structure of catalysts before and after FT synthesis. Powder X-ray diffraction patterns were recorded on a diffractometer (D8 DISCOVER, Bruker, Germany) with a monochromated CuKα radiation generated at 40 mA and 40 kV. The measurement was conducted at a room temperature with 2θ range of 20- 80° using a step counting time of 2 s and step size of 0.02°. The phase identification was done by comparing data of the peaks with the Powder Diffraction Files (PDF) obtained from the international centre for diffraction data (ICSD) database.

SEM-EDX measurements were carried out on a Zeiss EVO LS10 scanning electron microscope equipped with an Oxford INCA x-act energy dispersive X-ray spectrometer operated with an accelerating voltage of 15 kV. The ICP analysis of samples was conducted using a Varian 710-ES ICP-OES system.

2.3. Evaluation of catalytic Fisher-Tropsch synthesis

FT synthesis experiments were carried out in a tubular fixed bed reactor (7.8 mm inside diameter and 15.24 mm length). To ensure an isothermal condition along the reaction bed, the catalyst was mixed with SiC in 1:6 volumetric ratio (catalyst : SiC). Prior to the reaction, the catalyst was in-situ reduced using H_2 at 30 ml/(min·g-cat STP), 350 °C and 0.1 MPa for 15 hours, and then syngas at a composition of H_2/CO=2 and 30 ml/(min·g-cat STP) for an additional 1 hour. Then

154 the reactor was cooled down to 300 °C, and pressurized to 2 MPa under a flow of nitrogen. Then
155 the feed gas was introduced into the reactor at 30 mL/(h·g-cat) STP. Four mass flow controllers
156 (SLA5850S, Brooks Instruments, USA) were used to independently adjust the flow rates of H_2,
157 CO, CO_2, and N_2 streams. All four gases were preheated and mixed inside a vaporizer-mixer
158 chamber prior to entering the reactor. A cold trap at 8°C was placed right after the reactor,
159 followed by a pneumatically-controlled back pressure valve.
160
161 The reactor effluent was periodically analyzed in an on-line GC equipped with two TCDs and
162 one FID (RGA G3445B, Agilent Technologies, USA). H_2 was analyzed using a dedicated TCD
163 while CO, CO_2, and N_2 were quantified on the second TCD. Non-condensable C_1-C_5
164 hydrocarbons and small amounts of non-condensed C_{6+} hydrocarbons were quantified using an
165 FID. The sampling valve inside the GC was heated and kept at a constant temperature of 100 °C
166 and pressure of 13.8 kPa for sampling consistency. The liquid, wax and oxygenated
167 hydrocarbons condensed in the cold trap were collected at the end of each experiment for the
168 calculation of mass balance and analyzed on a GC-FID-MS unit (GC7890B/MS5975C, Agilent
169 Technologies, USA) equipped with a methyl silicone capillary column (HP-5MS, 30 m, 0.25
170 mm, 0.25 μm). The carbon balance for all experiments was calculated within the accuracy of
171 100%±7%. The carbon selectivity for all oxygenates formed during the FTS reactions were
172 typically below 3% and thus oxygenates were excluded from the calculation of the product
173 selectivity. After each experiment, the spent catalyst was passivated using a gas mixture of
174 1%O_2/99%N_2 at 35 °C for 1 hour, then the O_2 concentration was gradually increased before
175 exposing the catalyst to the air.
176

For evaluating the performance of the synthesized catalysts, the composition of the model syngas was set at 54%H_2/10%CO/29%CO_2/7%N_2, which was determined as the typical composition of syngas produced by oxygen/steam gasification of biomass reported in the literature [4, 17]. N_2 was used as an internal standard for the GC analysis and the representative of inert components in the syngas. For analyzing the effect of syngas composition on the catalytic FT synthesis, both H_2-balanced and H_2-deficient syngas were used. As it requires 2 moles and 3 moles of H_2 to convert each mole of CO and CO_2 into the precursor of $–CH_2$, respectively through FT synthesis, the stoichiometric ratio of hydrogen to total carbon, $H_2/(2CO+3CO_2)$, should be one. However, as the syngas from biomass gasification is typically deficient in H_2 (e.g., 54%H_2/10%CO/29%CO_2/7%N_2), the ratio of H_2 to $2CO+3CO_2$ at 0.5 was used as the representative composition of H_2-deficient syngas.

3. Results and discussion

3.1. Surface area and pore size distribution of catalysts

Table 2 presents the surface area, pore volume, and average pore volume of calcined catalysts measured with the N_2 physisorption.

Table 2. Textural properties of calcined catalysts

Catalysts notation	surface area (m^2/g)	Pore volume (cm^3/g)	Average pore size (nm)
Fe-Cu-K	31.0	0.17	22.4
Fe-Cu-K-Al	153.6	0.20	5.1
Fe-Cu-K-Si	246.0	0.23	4.0
Fe-Cu-K-Si-Al	202.3	0.22	4.4

196 The Fe-Cu-K catalyst had rather low surface area (31 m^2/g). Incorporation of SiO_2 or Al_2O_3 or
197 both resulted in significant increase in the surface area and reduction in the average size of pores.
198 Introduction of SiO_2 or Al_2O_3 provides a rigid matrix that helps to prevent complete collapse of
199 the original pore structure of Fe_2O_3/FeOOH precipitates during subsequent calcination, thus
200 maintaining the original high surface area partially or completely [22]. As expected, the addition
201 of SiO_2 to an Fe-Cu-K-Si-Al catalyst, increases the surface area to a value in between the purely
202 SiO_2 and Al_2O_3 promoted catalysts.
203
204 ### *3.2. Elemental composition*
205 The elemental compositions of fresh catalysts were analyzed using the EDX and ICP-OES
206 techniques. As given in Table 1, the elemental compositions of all catalysts measured by the ICP
207 were close to the corresponding values in the synthesis solutions. The compositions calculated
208 using the EDX, however, were significantly different from the bulk compositions measured by
209 the ICP, because the EDX typically measures the near-surface composition due to its limited
210 depth of penetration. It can be seen that the Al and Si concentrations were underestimated in
211 EDX while K was overestimated compared with the results of ICP analysis. Interestingly, the K
212 concentrations on the surface were the highest in Al_2O_3 containing samples, which were 5.6 and
213 5.1 atoms of K per 100 atoms of Fe for Al_2O_3-SiO_2 doubly promoted and Al_2O_3 catalysts,
214 respectively. The higher surface concentrations of K on those Al_2O_3 containing samples were
215 probably due to the weaker interactions of K with SiO_2 and Al_2O_3 so that a higher amount of K
216 was available on the catalyst surface to presumably interact with Fe.
217
218 Figure 1-a shows the SEM micrograph of Fe-Cu-K-Si-Al catalyst. The EDX mapping was used

to analyze the elemental distribution of Fe, Cu, K, Si, and Al on this sample (Figure 1b-f). All elements were observed to be uniformly distributed.

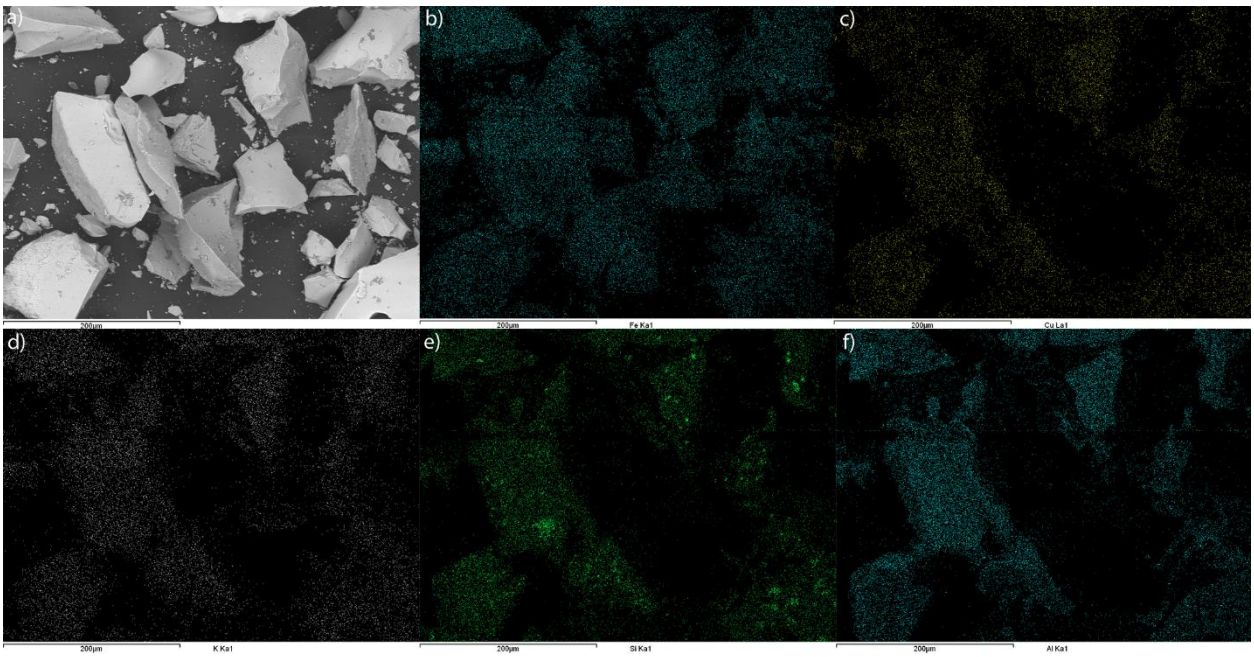

Figure 1. SEM micrograph and EDX mapping of Fe-Cu-K-Si-Al catalyst

3.3. H_2-TPR

The results for the reduction behavior of catalysts are given in Figure 2 and Table 3. The reduction profile of Fe-Cu-K catalyst was identical to that of pure Fe_2O_3 [23]. Besides the first reduction peak at around 280 °C related to the reduction of copper oxide to Cu, three reduction peaks due to the reduction of Fe_2O_3 to metallic Fe were observed according to the following reactions:

$$CuO + H_2 \rightarrow Cu + H_2O$$

$$3Fe_2O_3 + 3H_2 \rightarrow 2Fe_3O_4 + H_2O$$

$$Fe_3O_4 + H_2 \rightarrow FeO + H_2O$$

$$FeO + H_2 \rightarrow Fe + H_2O$$

231

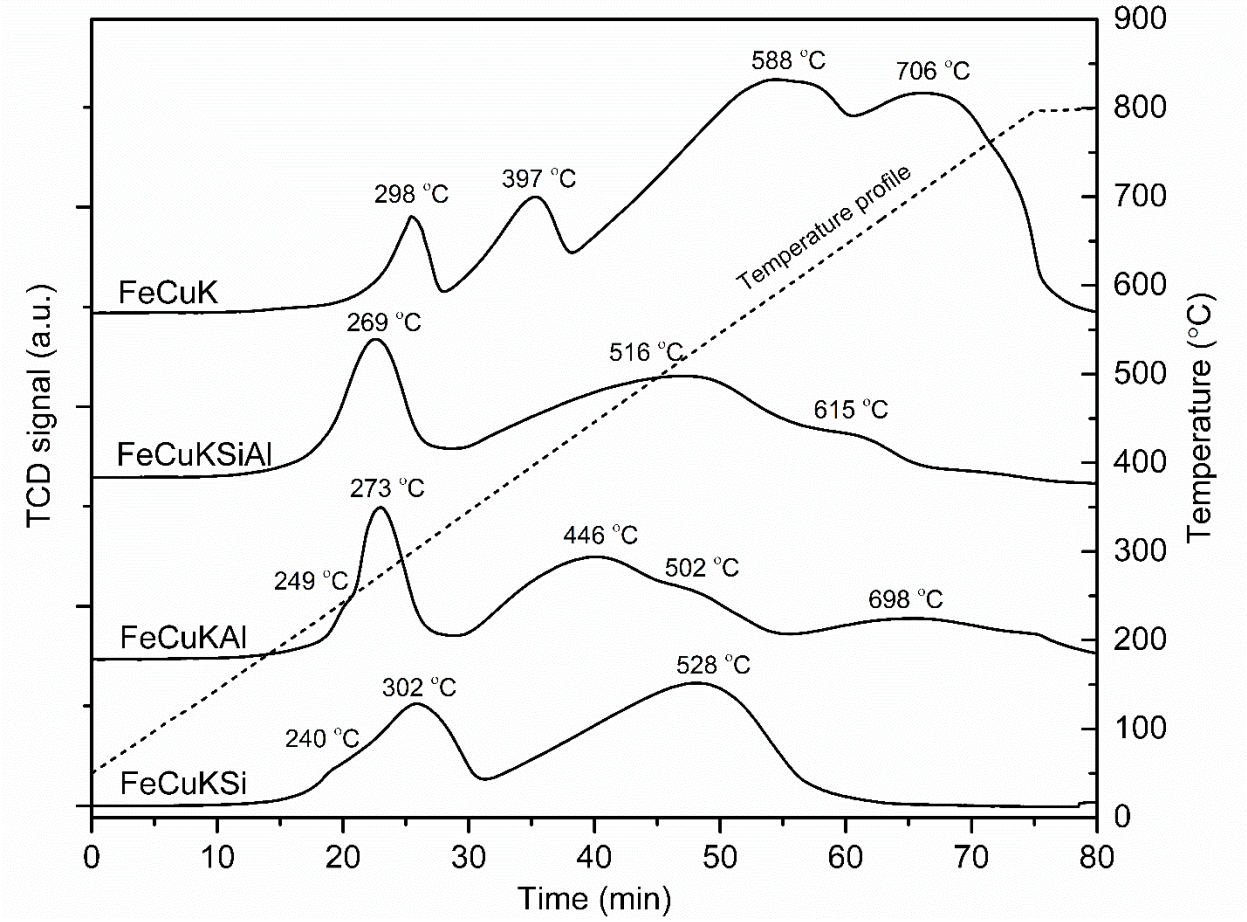

232

233 ***Figure 2. H_2-TPR profiles of fresh catalysts***

234 ***Table 3. Quantitative results of H_2-TPR and TPDC experiments***

Catalyst	H_2 consumption in TPR mole-H_2/mole-Fe	Extent of carburization [a]
Fe-Cu-K	0.89	100%
Fe-Cu-K-Al	0.72	88.6%
Fe-Cu-K-Si	0.71	20.9%
Fe-Cu-K-Si-Al	0.74	95.6%

235 [a] *Calculated by integrating the peak areas in Figure 4 and normalizing with the assumption of*

236 *100% carburization for the Fe-Cu-K catalyst*

Although it is well-known that the addition of Cu can facilitate the reduction of hematite to magnetite [24], Cu could not effectively facilitate Fe reduction in Fe-Cu-K catalyst probably because of the weak interaction between Cu and Fe. In other three catalysts, on the other hand, the addition of alumina and silica was favorable as the temperatures required for the reduction of both iron oxide and copper oxide to their metallic counterparts were significantly reduced. One reason could be that the introduction of a structural promoter such as alumina and silica improves the dispersion of iron crystallites as demonstrated by the BET results, leading to the better contact between Fe and Cu phases, and higher effectiveness of Cu promotion. A small shoulder around 240 °C on the reduction profiles of both alumina and silica is attributed to the reduction of CuO to Cu [24]. This shoulder was not observed in doubly-promoted catalyst probably because it was overlapped with the wide Fe_2O_3 reduction peak at 269 °C. The addition of Si to the Fe-Cu-K-Si-Al catalyst facilitated the reduction of iron oxide as the reduction of the catalyst was completed at lower temperature than that of Fe-Cu-K-Al catalyst. The Fe-Cu-K-Si-Al catalyst also exhibited the highest degree of reduction among all three SiO_2 and/or Al_2O_3 promoted catalysts (Table 3). From the TPR results, the simultaneous addition of SiO_2 and Al_2O_3 to Fe-Cu-K catalyst complex is advantageous in term of reduction behavior. This could be due to the increased surface area, better dispersion of Fe and Cu, and reduced metal-support interaction.

3.4. CO_2-TPD

Effect of the addition of SiO_2 and/or Al_2O_3 on the surface basicity was characterized by the CO_2-TPD, which is presented in Figure 3. A low temperature peak around 100 °C attributed to the weak adsorption of CO_2 was observed on all samples. In general, the addition of structural

promoters reduced the surface basicity as the intensity of CO_2 desorption profiles and the number of desorption peaks were decreased compared with the base Fe-Cu-K catalyst. This was caused by the interaction of Fe with Al_2O_3 and/or SiO_2 which reduced the effective amount of Fe to interact with CO_2. The addition of structural promoters also slightly intensified the high temperature desorption peak around 900 °C which was more sound for the doubly promoted and SiO_2 promoted catalysts. It is known that CO_2 is can be adsorbed on both Fe and alkali metal surfaces [9]. As K is a stronger base than Fe, it tends to adsorb CO_2 more strongly than Fe. So it is possible that the strong basic sites on SiO_2 and/or Al_2O_3 supported catalysts at 900 °C were caused by the higher dispersion of K. This was verified by the surface composition from the EDX analysis.

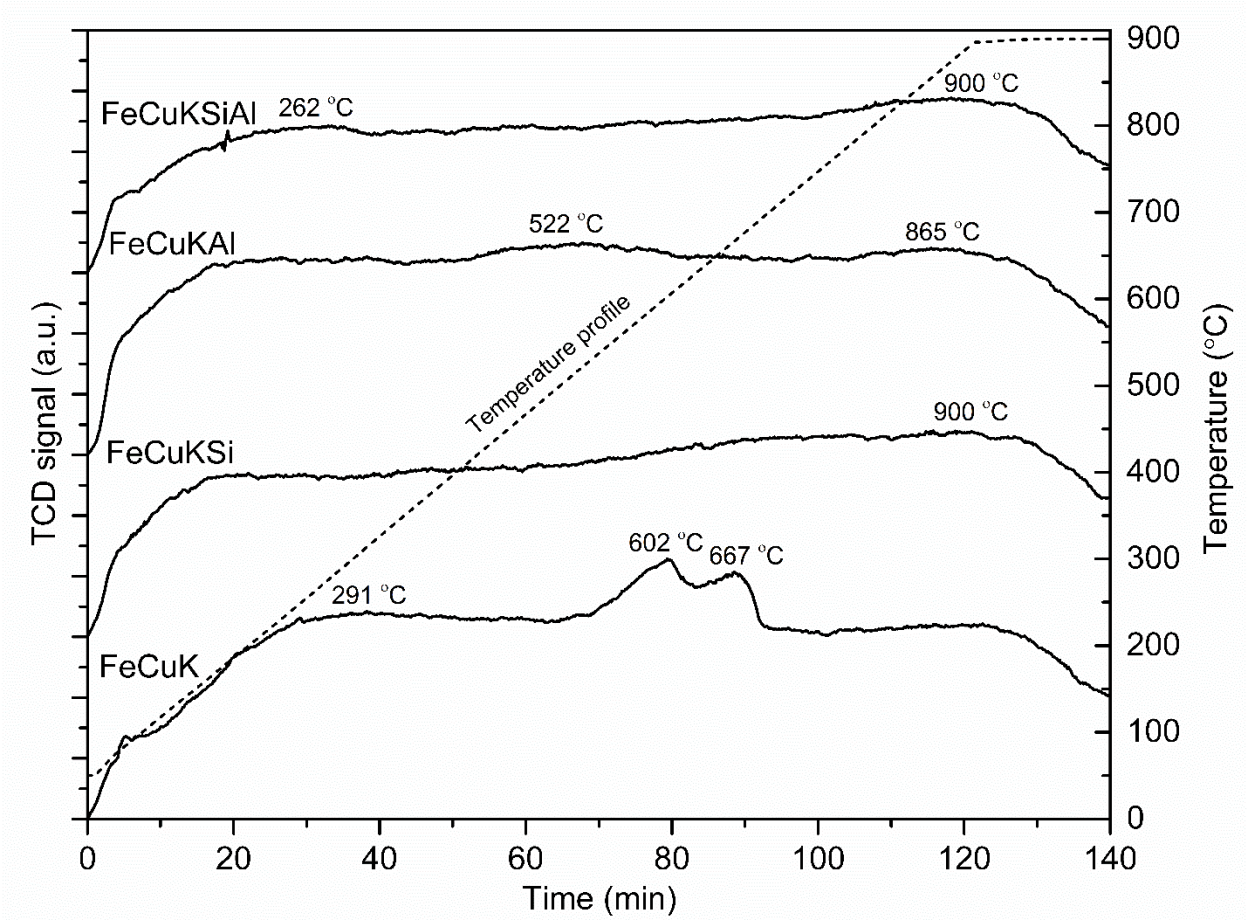

Figure 3. CO_2-TPD profiles of reduced catalysts

3.5. Crystalline structures of catalysts

Figure 4-a shows the XRD patterns of fresh samples. The XRD pattern of Fe-Cu-K base catalyst shows the formation of well-crystallized hematite phase with peaks identified at 2θ=24.1°, 33.1°, 35.7°, 40.9°, 49.5°, 54.1°, 57.5°, 62.4°, 64°, 71.9°, and 75.5°. In contrast, all Al_2O_3 and/or SiO_2 promoted catalysts, exhibited two broad peaks at 2θ values around 63° and 35°, which corresponded to small crystallites of iron oxide [25]. This indicates that the addition of SiO_2 and Al_2O_3 reduced the size of iron crystalline. It was reported that both Al_2O_3 and SiO_2 can improve the dispersion of iron oxide and prevents the aggregation of crystallites during the heat treatment of the freshly synthesized catalyst [26, 27].

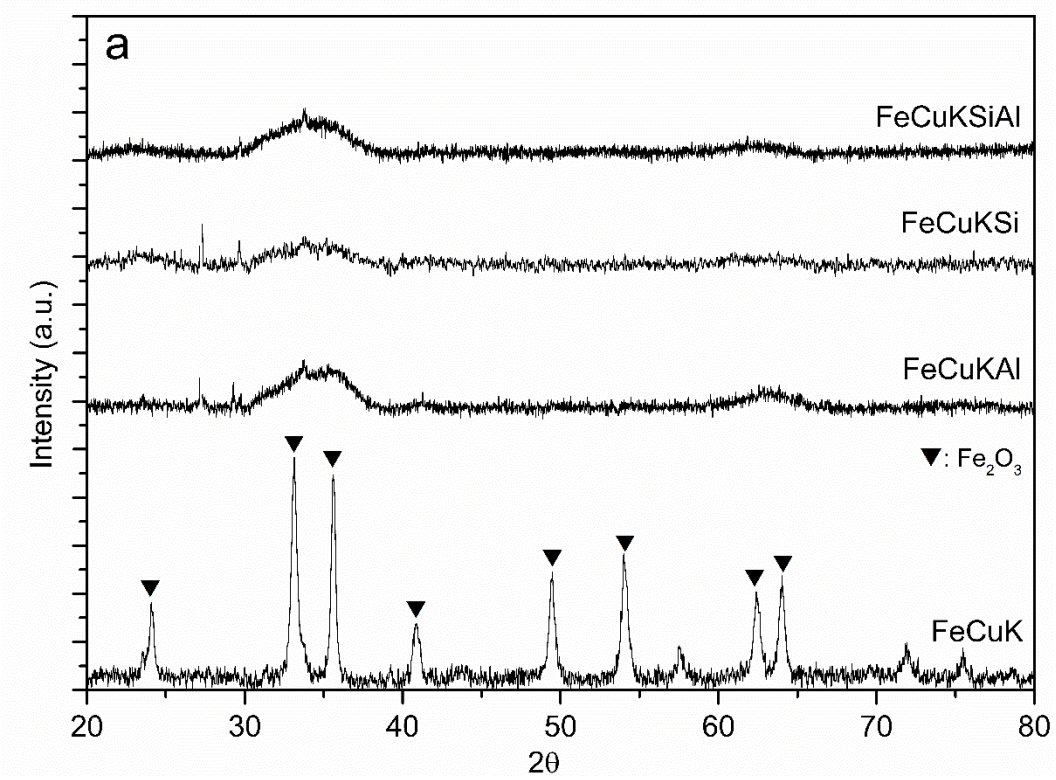

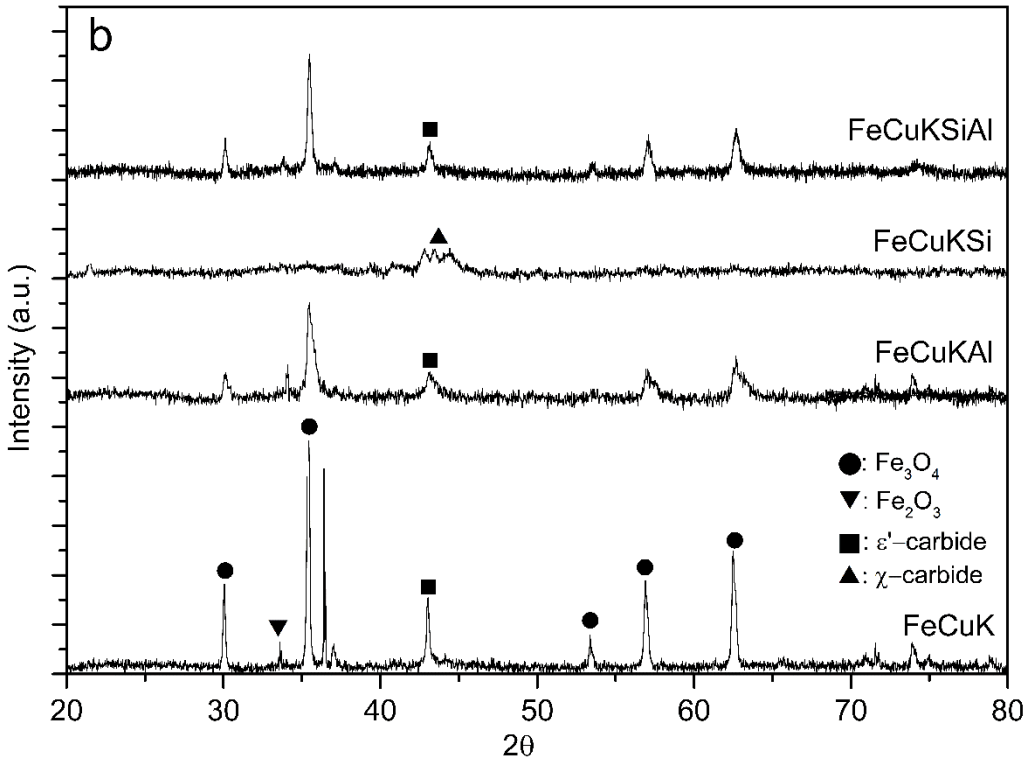

Figure 4. XRD patterns for a) fresh and b) used catalysts

The diffraction patterns of the used catalysts are shown in Figure 4-b. The ε'-carbide phase ($Fe_{2.2}C$) with a characteristic peak at the 2θ value around 43.2° was observed on all catalysts except Fe-Cu-K-Si catalyst. The ε'-carbide is believed to be more active in FTS than other carbide phases [16, 28]. On contrary, less active χ-carbide ($Fe_{2.5}C$) was detected on Fe-Cu-K-Si. It is possible that high CO_2 concentration of syngas used in this study hindered the transformation of χ-carbide into ε'-carbide in the Fe-Cu-K-Si [16].

3.6. Effect of SiO_2 and Al_2O_3 promotion on the FTS activity and selectivity

Table 4 shows the effect of the addition of SiO_2 and/or Al_2O_3 on the activity and selectivity of Fe-Cu-K catalyst system in the hydrogenation of the model biomass-derived syngas. The Fe-Cu-

297 K catalyst showed high activity for the hydrogenation of CO/CO_2 mixture without the addition of
298 any structural promoter. In a harsh operating environment of industrial FT synthesis, however,
299 the addition of support is desirable to improve the structural integrity and attrition resistance of
300 this catalyst. Interestingly, both doubly promoted SiO_2-Al_2O_3 and Al_2O_3 promoted catalysts
301 showed higher CO conversion (89.6% and 88.3%, respectively) than Fe-Cu-K (81.8%). This is
302 probably due to the higher dispersion of active metals and higher surface area on these two
303 samples (see Table 2). The doubly-promoted catalyst also achieved the highest CO_2 conversion
304 among all catalysts, which was 25.2%. The increase in CO_2 conversion was attributed to the
305 improved (R)WGS activity of the doubly promoted catalyst due to better dispersion of
306 potassium. Potassium is known to improve the rate of (R)WGS in Fe-based catalysts [29, 30].
307 The Fe-Cu-K-Si achieved the lowest CO conversion at 67.1% but relatively high CO_2
308 conversion. This can be explained by considering the occurrence of FT and WGS reactions on
309 different active sites on an iron catalyst.
310 Several authors have reported that magnetite phase (Fe_3O_4) is active for the WGS reaction,
311 whereas the FT reaction proceeds over carbidic phases [11, 31-35]. The XRD analysis of the
312 spent catalysts confirmed the presence of dominantly χ-carbide phase on the Fe-Cu-K-Si
313 catalyst, while other catalysts contained ε'-carbide phase which is more active for FTS.
314 Moreover, 13.2% of CO_2 conversion and 67.1% of CO conversion for this Fe-Cu-K-Si catalyst
315 was much higher than -1.6% of CO_2 conversion and 20.6% of CO conversion obtained at similar
316 reaction conditions reported in the literature [17]. The co-precipitation method of incorporating
317 SiO_2 into the catalyst as well as the nature of Si source (TEOS) used in this study might also
318 contribute to higher CO and CO_2 conversion than binder-added SiO_2 used in the literature.
319 Similarly, higher CO and CO_2 conversions (82.78% and 0.26%, respectively) were achieved for

the Fe-Cu-K-Al catalyst used in this study. Yang et al. (2005) [19] studied two different iron catalysts with SiO_2 added through precipitation and binder mixing. They reported that the addition of SiO_2 through co-precipitation resulted in higher hydrogenation activity and higher selectivity toward long-chain hydrocarbons. SiO_2 incorporated through the precipitation interacts more strongly with iron, enhancing the effectiveness of the potassium in the catalyst which can also have a positive effect on the selectivity of longer chain hydrocarbons.

Table 4. FT synthesis over iron-based catalysts with biomass-derived syngas [a]

Catalyst	CO conversion (%)	CO_2 conversion (%)	Hydrocarbon selectivity [b] (mole-C %)			Olefin selectivity %	
			CH_4	C_2-C_4	C_{5+}	C_2-C_4	C_5
Fe-Cu-K	81.8	18.5	5.9	18.6	75.5	89.0	81.0
Fe-Cu-K-Al	88.3	12.5	6.9	25.4	67.7	90.0	81.0
Fe-Cu-K-Si-Al	89.6	25.2	7.6	20.5	71.9	81.8	77.3
Fe-Cu-K-Si	67.1	13.2	13.9	18.6	67.4	89.0	82.6

a Reaction condition: (54%H_2/10%CO/29%CO_2/7%N_2), 300 °C, 2 MPa, and 30 mL/(min·g-cat) for 72 h TOS

b an CO_2-free basis

The selectivity of liquid hydrocarbons (C_{5+}) was the highest at 75.5% using the Fe-Cu-K catalyst. This catalyst produced the lowest amount of methane (5.9%) and gaseous (C_2-C_4) hydrocarbons (18.6%). This might be attributed to the higher surface basicity of this catalyst, as evidenced by the results of our CO_2-TPD experiment. The higher surface basicity is known to favor the production of higher molecular weight hydrocarbons [22, 30, 36]. All three supported catalysts, in contrast, produced slightly more methane and light hydrocarbons and less liquid hydrocarbons (C_{5+}). It is reported that the addition of SiO_2 or Al_2O_3 retards the surface basicity on iron based catalysts [19, 25, 27] resulting in the production of lower molecular weight hydrocarbons. Among all Si and/or Al promoted catalysts, the doubly promoted catalyst had the highest liquid hydrocarbon selectivity (C_{5+}) at 71.9%. This could be attributed to the better

dispersion of potassium on this catalyst compared to other promoted catalysts. Potassium is known to improve the surface basicity and thus the selectivity of longer chain hydrocarbons [22, 37]. The Fe-Cu-K-Si catalyst showed the highest methane selectivity (13.9%) and slightly lower liquid hydrocarbons (67.4%) among all promoted catalysts. This is because SiO_2 tends to have more acidic characteristics than Al_2O_3 [38].

3.7. Effect of CO_2 content on FTS activity and selectivity

Tables 5 and 6 give the conversion efficiency and hydrocarbon selectivity of FT synthesis over Fe-Cu-K-Si-Al catalyst with varying $CO_2/(CO+CO_2)$ ratio in H_2-deficient and H_2-balanced conditions, respectively.

In both H_2-deficient and H_2-balanced conditions, the CO conversion was higher than 98% for the syngas with H_2 and CO only, i.e., $CO_2/(CO+CO_2)=0$, while the CO conversion decreased with the increase of $CO_2/(CO+CO_2)$ ratio from 0.25 to 0.75. This might be caused by more CO generated through the rWGS reaction at higher $CO_2/(CO_2+CO)$ ratios [39]. In both H_2-deficient and H_2-balanced conditions, CO_2 was also converted to hydrocarbons when the concentration of CO_2 was higher than a certain value (i.e., 0.35 for H_2-balanced syngas, and 0.5 for H_2-deficient syngas). The conversion of CO_2 to FT products proceeds via a two-step process: 1) reaction of CO_2 with H_2 to produce water and CO, and 2) FT reaction of generated CO with H_2 to produce hydrocarbons. When the conversion of CO_2 is zero, the net rate of formation and consumption of CO_2 through the WGS reaction is zero. The lower $CO_2/(CO_2+CO)$ ratio at which the CO_2 conversion is zero, the higher activity of the catalyst for the reverse rWGS reaction during the FT synthesis.

Table 5. FT synthesis over Fe-Cu-K-Si-Al catalysts with H_2-deficient syngas [a]

CO_2/(CO+CO_2)	CO conversion (%)	CO_2 conversion (%)	CO_2 selectivity	CO selectivity	Hydrocarbon selectivity (mole-C %)			Olefin selectivity %	
					CH_4	C_2-C_4	C_{5+}	C_2-C_4	C_5
1.0	-	40.7	-	5.8	5.4	15.9	78.7	70.0	83.5
0.75	89.6	25.2	-	-	7.6	20.5	72.0	72.7	81.8
0.5	88.7	0	-	-	10.2	24.7	65.1	79.2	79.2
0.25	95.9	-83.7	-	-	11.5	25.9	62.6	75.8	76.7
0	98.0	-	39.2	-	11.7	24.2	64.2	73.7	76.5

a Reaction condition: H_2-deficient syngas (H_2/(2CO+3CO_2)=0.5), 300 °C, 2 MPa, and 30 mL/(min·g-cat) for 72 h TOS

Table 6. FT synthesis over Fe-Cu-K-Si-Al catalysts with H_2-balanced syngas [a]

CO_2/(CO+CO_2)	CO conversion (%)	CO_2 conversion (%)	CO_2 selectivity	CO selectivity	Hydrocarbon selectivity (mole-C %)			Olefin selectivity %	
					CH_4	C_2-C_4	C_{5+}	C_2-C_4	C_5
1.0	-	50.1	-	3.6	9.8	26.0	64.2	64.1	78.2
0.75	93.1	40.5	-	-	10.4	27.0	62.6	62.7	77.3
0.5	97.1	28.4	-	-	12.7	29.0	58.2	76.5	74.1
0.35	97.3	4.0	-	-	13.6	30.8	55.7	73.4	74.5
0.25	98.1	-38.7	-	-	14.1	30.2	55.7	75.3	71.9
0	98.6	-	30.3	-	14.7	29.2	56.1	73.4	73.3

a H_2-balanced syngas (H_2/(2CO+3CO_2)=1.0), 300°C, 2 MPa, and 30 mL/(min·g-cat) for 72 h TOS

As seen in Table 7, the Fe-Cu-K-Si-Al catalyst in this study exhibited superior activity in FT synthesis from a CO_2-containing syngas, which achieved positive CO_2 conversion at much lower CO_2/(CO_2+CO) ratios than data reported in the literature. As CO_2 might be converted into FT products over an Fe-based catalyst, it would be beneficial to keep some CO_2 in the syngas prior to entering the conversion reactor to suppress the formation of CO_2 through WGS reaction and to supply additional carbon source for the synthesis of hydrocarbons. This is more important when syngas is generated through the gasification of biomass, coal, and bio-oil as it would contain a

significant amount of CO_2 [4, 40].

Table 7. Minimum $CO_2/(CO+CO_2)$ ratio in syngas for positive CO_2 conversion during FT synthesis

Catalyst	$CO_2/(CO+CO_2)$	Syngas composition ($H_2/CO/CO_2$/inert)	Condition remarks	Ref.
Fe/TiO_2	0.75	H_2-balanced 69%/5.25%/15.75%/10%[a]	60 mL/min·g-cat, T=250°C, P=2 MPa bar, X_{CO} ~81%[a]	[14]
Fe-Cu-K-Al	0.45[a]	H_2-reach bio-oil syngas	T=260°C, P=15 bar X_{CO} ~90%[a]	[40]
Fe-Cu-K-Al	0.43	H_2-balanced $H_2/(2CO+3CO_2)=1$	30 mL/min·g-cat, T=300°C, P=2 MPa, X_{CO}>95%	[39, 43]
Fe-Cu-K-Al	0.74	H_2-deficient 52%/11%/32%/5%	30 mL/min·g-cat, T=300°C, P=1 MPa, X_{CO}=82.8%	[17]
Fe-Cu-K-Si-Al	0.35	H_2-balanced 65%/18%/10%/7%	30 mL/min·g-cat, T=300°C, P=2 MPa, X_{CO}>95%	This work
Fe-Cu-K-Si-Al	0.50	H_2-deficient 53%/20%/20%/7%	30 mL/min·g-cat, T=300°C, P=2 MPa, X_{CO}>95%	This work

a data are extracted by interpolation from the plots

The selectivity of the Fe-Cu-K-Si-Al catalyst towards liquid hydrocarbons (C_{5+}) increased with the $CO_2/(CO+CO_2)$ ratio at the expense of decrease in CH_4 selectivity. A similar trend was reported by other researchers [39, 41]. At high CO_2 concentrations, the WGS reaction is shifted to the reverse direction, which increases the amount of water generated. As water inhibits the hydrogenation reaction, the increase of water concentration inside the reactor will increase the probability of hydrocarbon chain propagation and also suppress the methanation reaction [42]. The syngas with CO_2 as an only carbon source, i.e., $CO_2/(CO+CO_2)=1$, achieved the lowest methane selectivity. In this case, methane selectivity was only 5.4% and 9.8% for H_2-deficient and H_2-balanced syngas, respectively (Tables 5 and 6).

3.8. Comparison between the catalyst activity and product selectivity for H_2-deficient and H_2-balanced syngas

CO and CO_2 reactivity. In the hydrogenation of CO and a CO/CO_2 mixture, the conversion of CO increased as the $H_2/(CO+CO_2)$ ratio increased for all $CO_2/(CO+CO_2)$ ratios (Tables 5 and 6), which was consistent with the data reported by Yali et al. [14]. The increase of $H_2/(2CO+3CO_2)$ ratio also improved the CO_2 conversion in syngas with all $CO_2/(CO+CO_2)$ ratios. As the addition of H_2 will shift the equilibrium of the following WGS reaction to the left side, more CO_2 will be converted to CO and subsequently to FT hydrocarbons.

$$CO + H_2O \leftrightarrow CO_2 + H_2 \qquad (WGS\ reaction)$$

Products selectivity. As given in Tables 5 and 6, the increase of hydrogen content in the syngas increased the methane selectivity at the expense of decrease in the liquid hydrocarbons selectivity. It was also reported in the literature that the selectivity towards long-chain hydrocarbons decreases with an increase of the H_2/CO ratio in the feed gas [11, 37, 44]. The increase of the hydrogen partial pressure will decrease the probability of hydrocarbon chain-growth and thus increase the probability of the termination of a growing hydrocarbon chain, which results in the formation of more shorter-chain hydrocarbons as well as a higher fraction of saturated products. The increase of $H_2/(2CO+3CO_2)$ ratio of the syngas with different $CO_2/(CO+CO_2)$ ratios increases the methane selectivity. The methane selectivity increased from 5.4% under H_2-deficient environment (i.e., $H_2/(2CO+3CO_2)=0.5$) to 9.7% under H_2-balanced environment (i.e., $H_2/(2CO+3CO_2)=1.0$) for the syngas with H_2 and CO_2 only. This was the highest increase in the methane selectivity observed in all experiments by switching from H_2-deficient to H_2-balanced syngas. Yao et al. (2011) reported similar effect of H_2 concentration on

420 the methane selectivity of CO_2 hydrogenation [14]. The methane selectivity for the syngas with
421 H_2 and CO was 11.7% for H_2-deficient condition and 14.7% for H_2-balanced condition, which
422 were significantly higher than those of the syngas with H_2 and CO_2.
423
424 When the syngas contains only CO and H_2, CO_2 is a one of the products during the Fe-catalyzed
425 FT synthesis due to the WGS reaction [11]. In this case, the CO_2 selectivity was 39.2% at the H_2-
426 deficient condition (i.e., H_2/CO=1.0) and 30.3% at the H_2-balanced condition (i.e., H_2/CO=2.0).
427 Therefore, 39.2% and 33.3% of carbon (CO) in the syngas was converted to CO_2 during the FT
428 synthesis at H_2-deficient and H_2-balanced conditions, respectively. The increase of H_2 content in
429 the syngas can inhibit the WGS reaction in the forward direction, thus reducing the amount of
430 CO_2 generated.
431

432 *3.9. Temperature programmed decarburization of spent catalysts in H_2*

433 The temperature programmed decarburization with H_2 was performed on spent catalysts to
434 determine the relative amount and stability of iron-carbide phases formed during FT reaction
435 (Figure 5). There were two groups of high temperature and low temperature peaks on the TPDC
436 profile of the Fe-Cu-K catalyst: a single low-temperature peak at 265 °C, and two high-
437 temperature peaks at 496 °C and 584 °C. The low and high temperature peaks were attributed to
438 the surface and bulk iron carbides, respectively [12]. For the Fe-Cu-K-Si catalyst with the SiO_2
439 promoter, the temperature and intensity of high-temperature peaks decreased, compared to the
440 Fe-Cu-K catalyst. The addition of the Al_2O_3 promoter to form Fe-Cu-K-Al and Fe-Cu-K-Si-Al
441 catalysts led more intensive carburization and stable iron-carbide phases with increased peak
442 temperature than the Fe-Cu-K-Si catalyst during the FT reaction. As seen in Figure 3 and Table

3, the structural promoters (SiO_2 and Al_2O_3) reduced the amounts of carbides formed on the catalysts during the FT synthesis, which was determined by calculating the peak areas of TPDC profiles. This should be due to the metal-support interactions which reduces reducibility and carburization of iron. Moreover, a correlation between FTS activity with the amount of carbon formed during the reaction was observed on all promoted catalysts. Among all three promoted catalysts, the doubly-promoted catalyst (Fe-Cu-K-Si-Al) showed the highest degree of carburization (Table 3). The doubly-promoted catalyst might have a higher degree of dispersion of Fe and K which increased the effectiveness of K promotion to enhance the carburization of Fe-based catalyst [9, 12]. The better dispersion of catalyst active phases due to simultaneous addition of SiO_2 and Al_2O_3 was also reflected by the TPR data (Figure 1 and Table 3). The lowest amount of carbide phase was formed when the Fe-Cu-K-Si catalyst was used. The XRD results confirmed that high CO_2 concentration in syngas might suppress the formation of more active iron-carbide phase (ε'-carbide) and promote the formation of less active iron phase (χ-carbide) on the SiO_2 promoted catalyst.

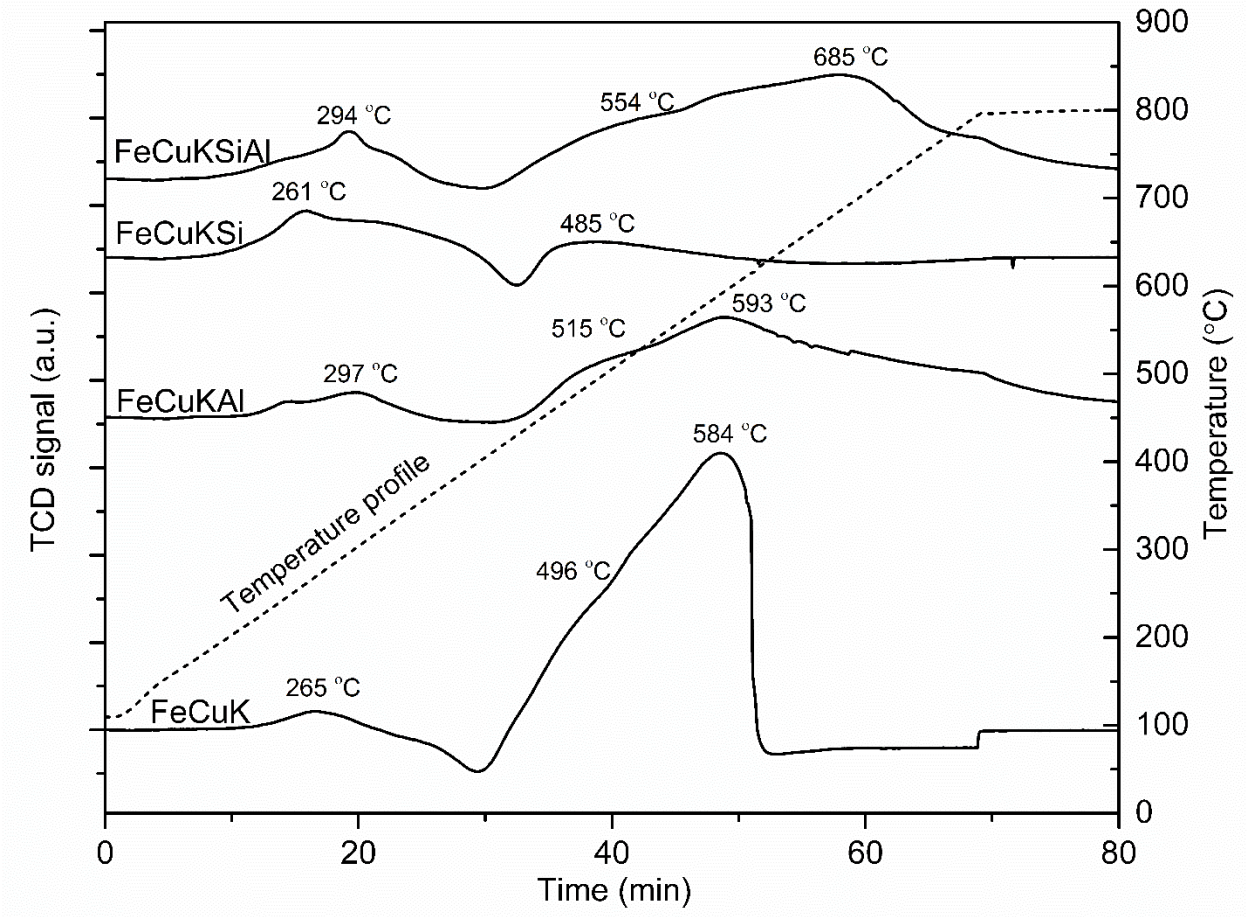

457

458 ***Figure 5. TPDC profiles of catalysts after FTS reaction***

459

460 # 4. Conclusion

461 The structural promoters of SiO_2 and Al_2O_3 had significant effects on the activity and selectivity
462 of the Fe-Cu-K based catalyst for FT synthesis with a model biomass-derived syngas. The
463 simultaneous addition of silica and alumina to Fe-Cu-K catalyst resulted in better dispersion of
464 Fe and Cu, and K. The doubly-promoted catalyst (Fe-Cu-K-Si-Al) achieved higher CO and CO_2
465 conversions than Fe-Cu-K catalyst and singly-promoted Fe-Cu-K-Al and Fe-Cu-K-Si catalysts.
466 The CO and CO_2 conversions for doubly-promoted catalyst were 88.3% and 25.2%, respectively,
467 for the syngas with a composition of 54%H_2/10%CO/29%CO_2/7%N_2, compared to 81.8% and

18.5% for the Fe-Cu-K catalyst. The C_{5+} selectivity of the doubly-promoted catalyst was 71.9%, which was slightly lower than 75.5% for the Fe-Cu-K catalyst, due to the decreased surface basicity. The SiO_2 promoted catalyst had the lowest CO conversion due to the suppressed formation of highly active carbide phase during the FTS with CO_2-rich syngas. The H_2 to carbon (CO and CO_2) ratio in the feed gas affects both carbon conversion efficiency and product selectivity of FT synthesis. The increase of the H_2 to carbon ratio in the syngas significantly increased the carbon conversion efficiency, and slightly increased the selectivity of methane and shorter-chain hydrocarbons at the expense of the decrease in the selectivity of longer-chain hydrocarbons. In both H_2-deficient and H_2-balanced conditions, CO_2 was converted to hydrocarbons during FT synthesis with the doubly-promoted catalyst when the concentration of CO_2 was higher than a certain value (i.e., 0.35 for H_2-balanced syngas, and 0.5 for H_2-deficient syngas). The increase of hydrogen content in the syngas increased the methane selectivity at the expense of decrease in the liquid hydrocarbon selectivity. The methane selectivity increased from 5.4% under H_2-deficient environment (i.e., $H_2/(2CO+3CO_2)=0.5$) to 9.7% under H_2-balanced environment (i.e., $H_2/(2CO+3CO_2)=1.0$) for the syngas with H_2 and CO_2 only. The methane selectivity for the syngas with H_2 and CO was 11.7% for H_2-deficient condition and 14.7% for H_2-balanced condition, which were significantly higher than those of the syngas with H_2 and CO_2.

Acknowledgements

A contribution of North Carolina Agricultural and Technical State University, supported by funds partially provided by U.S. Department of Energy (Grant#: EE0003138) and U.S National Scientific Foundation (Grant #: HRD-1242152). Mention of a trade name, proprietary products,

491 or company name is for presentation clarity and does not imply endorsement by the authors or
492 the university.

493 References

494 [1] L.M.D. Pravat K. Swaina, S.N. Naikb, Renewable and Sustainable Energy Reviews 15 (2011)
495 4917–4933.
496 [2] M.F. Demirbas, Applied Energy 86 (2009) S151–S161.
497 [3] S. Mehta, V. Deshmane, S. Zhao, D. Kuila, Industrial & Engineering Chemistry Research 53
498 (2014) 16245-16253.
499 [4] Z.A.B.Z. Alauddin, P. Lahijani, M. Mohammadi, A.R. Mohamed, Renewable and Sustainable
500 Energy Reviews 14 (2010) 2852-2862.
501 [5] M.J.A. Tijmensen, A.P.C. Faaij, C.N. Hamelinck, M.R.M. van Hardeveld, Biomass and
502 Bioenergy 23 (2002) 129-152.
503 [6] K. Zhang, U. Kogelschatz, B. Eliasson, Energy & Fuels 15 (2001) 395-402.
504 [7] W. Ning, N. Koizumi, M. Yamada, Energy & Fuels 23 (2009) 4696-4700.
505 [8] O.O. James, A.M. Mesubi, T.C. Ako, S. Maity, Fuel Processing Technology 91 (2010) 136-
506 144.
507 [9] P. Choi, K.-W. Jun, S.-J. Lee, M.-J. Choi, K.-W. Lee, Catal Lett 40 (1996) 115-118.
508 [10] M. Iglesias, R. Edzang, G. Schaub, Catalysis Today 215 (2013) 194-200.
509 [11] G.P. Van Der Laan, A.A.C.M. Beenackers, Catalysis Reviews 41 (1999) 255-318.
510 [12] T. Riedel, M. Claeys, H. Schulz, G. Schaub, S.-S. Nam, K.-W. Jun, M.-J. Choi, G. Kishan, K.-W.
511 Lee, Applied Catalysis A: General 186 (1999) 201-213.
512 [13] M. Martinelli, C.G. Visconti, L. Lietti, P. Forzatti, C. Bassano, P. Deiana, Catalysis Today 228
513 (2014) 77-88.
514 [14] Y. Yao, X. Liu, D. Hildebrandt, D. Glasser, Industrial & Engineering Chemistry Research 50
515 (2011) 11002-11012.
516 [15] P.S. Sai Prasad, J. Bae, K.-W. Jun, K.-W. Lee, Catal Surv Asia 12 (2008) 170-183.
517 [16] T. Herranz, S. Rojas, F.J. Pérez-Alonso, M. Ojeda, P. Terreros, J.L.G. Fierro, Journal of
518 Catalysis 243 (2006) 199-211.
519 [17] K.-W. Jun, H.-S. Roh, K.-S. Kim, J.-S. Ryu, K.-W. Lee, Applied Catalysis A: General 259 (2004)
520 221-226.
521 [18] H. Wan, B. Wu, H. Xiang, Y. Li, ACS Catalysis 2 (2012) 1877-1883.
522 [19] Y. Yang, H.-W. Xiang, L. Tian, H. Wang, C.-H. Zhang, Z.-C. Tao, Y.-Y. Xu, B. Zhong, Y.-W. Li,
523 Applied Catalysis A: General 284 (2005) 105-122.
524 [20] F. Ding, A. Zhang, M. Liu, X. Guo, C. Song, RSC Advances 4 (2014) 8930-8938.
525 [21] H.-J. Wan, B.-S. Wu, C.-H. Zhang, B.-T. Teng, Z.-C. Tao, Y. Yang, Y.-L. Zhu, H.-W. Xiang, Y.-W.
526 Li, Fuel 85 (2006) 1371-1377.
527 [22] D.B. Bukur, X. Lang, D. Mukesh, W.H. Zimmerman, M.P. Rosynek, C. Li, Industrial &
528 Engineering Chemistry Research 29 (1990) 1588-1599.
529 [23] A.J.H.M. Kock, H.M. Fortuin, J.W. Geus, Journal of Catalysis 96 (1985) 261-275.
530 [24] S. Li, A. Li, S. Krishnamoorthy, E. Iglesia, Catal Lett 77 (2001) 197-205.

[25] H. Suo, C. Zhang, B. Wu, J. Xu, Y. Yang, H. Xiang, Y. Li, Catalysis Today 183 (2012) 88-95.
[26] H.-J. Wan, B.-S. Wu, Z.-C. Tao, T.-Z. Li, X. An, H.-W. Xiang, Y.-W. Li, Journal of Molecular Catalysis A: Chemical 260 (2006) 255-263.
[27] H.-J. Wan, B.-S. Wu, X. An, T.-Z. Li, Z.-C. Tao, H.-W. Xiang, Y.-W. Li, Journal of Natural Gas Chemistry 16 (2007) 130-138.
[28] D.H. Chun, J.C. Park, S.Y. Hong, J.T. Lim, C.S. Kim, H.-T. Lee, J.-I. Yang, S. Hong, H. Jung, Journal of Catalysis 317 (2014) 135-143.
[29] H. Schulz, Applied Catalysis A: General 186 (1999) 3-12.
[30] M.E. Dry, Catalysis: science and technology (J. R. Anderson and M. Boudart, eds.), Springer-Verlag, 1981.
[31] E.S. Lox, G.F. Froment, Industrial & Engineering Chemistry Research 32 (1993) 71-82.
[32] K.R.P.M. Rao, F.E. Huggins, V. Mahajan, G.P. Huffman, V.U.S. Rao, B.L. Bhatt, D.B. Bukur, B.H. Davis, R.J. O'Brien, Topics in Catalysis 2 (1995) 71-78.
[33] M.D. Shroff, D.S. Kalakkad, K.E. Coulter, S.D. Kohler, M.S. Harrington, N.B. Jackson, A.G. Sault, A.K. Datye, Journal of Catalysis 156 (1995) 185-207.
[34] D.S. Newsome, Catalysis Reviews 21 (1980) 275-318.
[35] H.-b. Zhang, G.L. Schrader, Journal of Catalysis 95 (1985) 325-332.
[36] R.B. Anderson, B. Seligman, J.F. Shultz, R. Kelly, M.A. Elliott, Industrial & Engineering Chemistry 44 (1952) 391-397.
[37] B. Jager, R. Espinoza, Catalysis Today 23 (1995) 17-28.
[38] L. Shirazi, E. Jamshidi, M.R. Ghasemi, Crystal Research and Technology 43 (2008) 1300-1306.
[39] S.C. Kang, K.-W. Jun, Y.-J. Lee, Energy & Fuels 27 (2013) 6377-6387.
[40] Z.X. Wang, T. Dong, L.X. Yuan, T. Kan, X.F. Zhu, Y. Torimoto, M. Sadakata, Q.X. Li, Energy & Fuels 21 (2007) 2421-2432.
[41] M.E. Dry, Product R&D 15 (1976) 282-286.
[42] C.N. Satterfield, R.T. Hanlon, S.E. Tung, Z.M. Zou, G.C. Papaefthymiou, Industrial & Engineering Chemistry Product Research and Development 25 (1986) 407-414.
[43] C. Zhang, K.-W. Jun, K.-S. Ha, Y.-J. Lee, S.C. Kang, Environmental Science & Technology 48 (2014) 8251-8257.
[44] G.P. van der Laan, A.A.C.M. Beenackers, Applied Catalysis A: General 193 (2000) 39-53.

Graphical Abstract

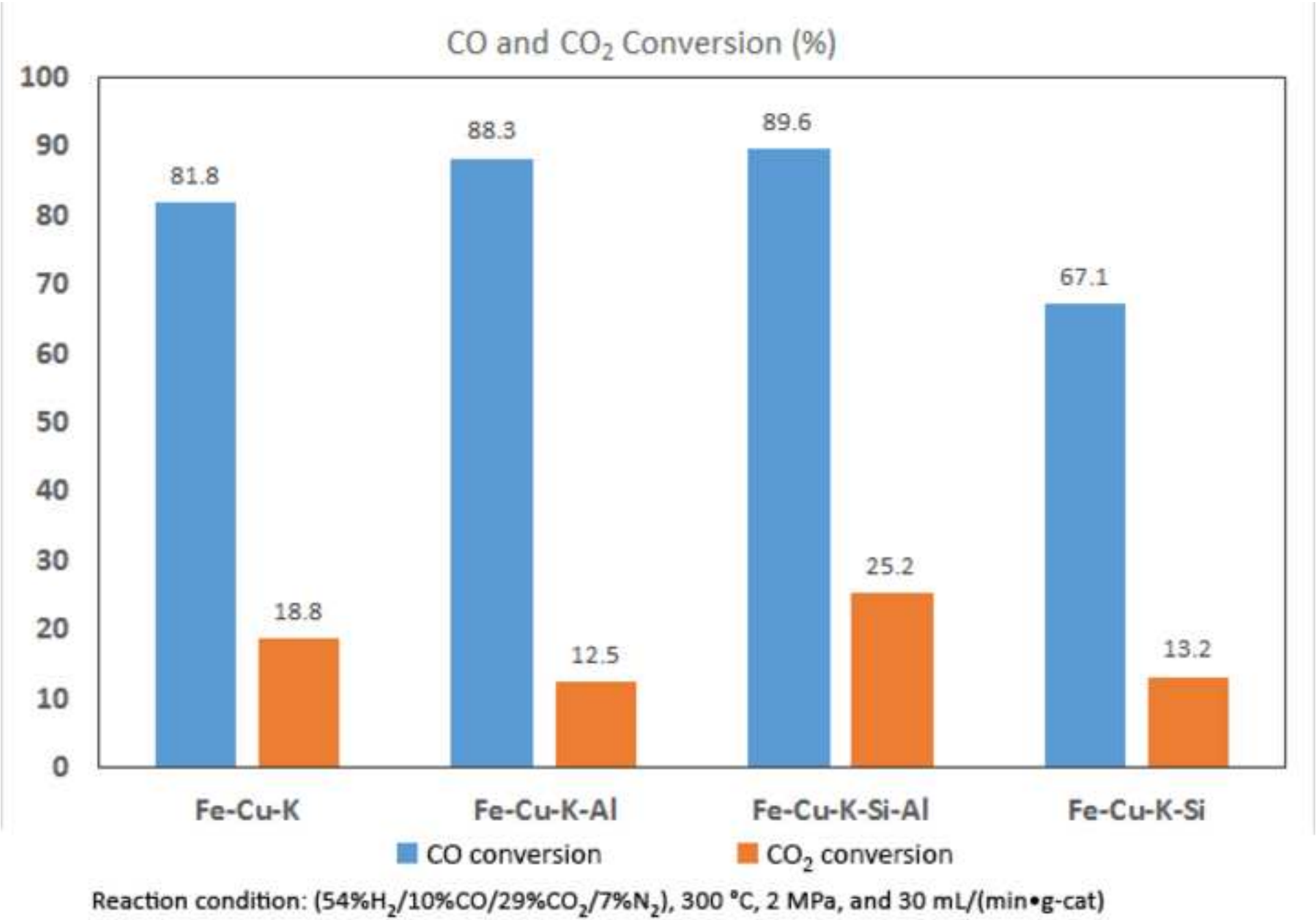

Reaction condition: (54%H_2/10%CO/29%CO_2/7%N_2), 300 °C, 2 MPa, and 30 mL/(min•g-cat)